dynaLYZE—an analysis package for time-series NIRS imaging data

Y. Pei[1], H. L. Graber[1,2], Y. Xu[1,2] and R. L. Barbour[1,2]

[1]NIRx Medical Technologies LLC / 15 Cherry Lane / Glen Head, NY 11545 / cschmitz@nirx.net, [2]Dept. of Pathology / SUNY Downstate Medical Center / 450 Clarkson Ave. Brooklyn, NY 11203

INTRODUCTION

DYnamic **N**ear-Infrared **O**ptical **T**omography, **DYNOT**, is a new noninvasive functional imaging method that employs low-intensity laser radiation to probe highly scattering media, such as tissue, in order to examine an entirely new class of information involving tissue function—the spatiotemporal dynamics of the vascular response [1]. *dyna*LYZE is a Matlab-based multifunctional analysis and visualization package specifically developed to support investigation of time-series data produced by the DYNOT imaging system, developed by NIRx in collaboration with SUNY. Functionalities include routines for detector pre-processing, image reconstruction, and time series analysis (e.g., time-frequency analysis, signal separation, time correlation and rate analysis), with each embedded within an versatile 2D/3D visualization package. *dyna*LYZE employs pull-down menus and data field entry to enable fast and efficient exploration of complex physiological phenomena.

*dyna*LYZE OVERVIEW

*dyna*LYZE basically supports three classes of analysis tools: Tools for pre-processing of raw, multiple-wavelength detector data, image reconstruction (μ_a, μ_s') from normalized multi-wavelength detector data, and post-processing of the detector/image data. A schematic of these operations and a flow diagram of their use is given in Figure 1.

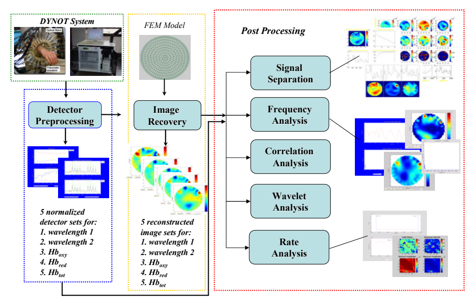

Figure 1. Overview of dynaLYZE software package.

MAIN FEATURES

General (Figure 2)

- Pull-down windows commands
- Integrated signal/image time series analysis software suite
- Signal/image frequency filtering (high-, low- or bandpass filter)
- Temporal signal/image ROI analysis
- Special point-and-click signal/image analysis

Image Recovery

- Finite element method (FEM) solver for diffusion equation
- 2D and 3D time series image reconstruction based on NMD and SVD
- User selectable FEM geometry library

Visualization

- Signal/Image temporal and special views
- Image animations
- Integrated display software (NIRx-GiD) allows
  - Multiple selectable viewing formats (isosurface, contour, vector, variable slice)
  - Interactive control of viewing presentation (zoom, pan, rotate, lighting)

Analysis tools

- Time-frequency analysis (Fourier transform, wavelet analysis, cross-spectral density, coherence)
- Time-correlation analysis (autocorrelation, cross-correlation)
- Temporal decomposition (principal component analysis, extended temporal decorrelation, GLM).
- Rate analysis (slope analysis, curve fitting and interval analysis)

DETECTOR PREPROCESS

The operations that fall under the **Detector Preprocess** code module are used to deal with raw detector data sets produced by DYNOT scanner. Three main functions are performed. First, the raw data for each source-detector pair (or channel) are corrected for fluctuations in laser power. Second, each channel's data are normalized to the temporal mean value during a user-specified baseline measurement period. Last, it converts the normalized multiple-wavelength data into relative changes in oxy-, deoxy- and total hemoglobin levels. The operation also provides functionalities of frequency pass filters and CV (coefficient of variation) calculation of coefficient of variation for those specified detector data sets based on the user-specified parameters during the process. A flowchart of the sequence of **Detector Preprocess** operations is shown in Figure 3.

IMAGE RECOVERY

Image Recovery operates on the normalized detector data sets that are the output of **Detector Preprocessing**. This code module performs two main functions. First it reconstructs sets of image time series from multiple- wavelength-based normalized detector data sets using a previously developed fast reconstruction algorithm [2], where an FEM is employed to solve diffusion-based forward-problem models to derive weight or Jacobian matrices, the inverse system equations is generated by means of normalized difference method (NDM) [3] and several scaling techniques, and singular value decomposition (SVD) is used to compute the image sequences for each data set. Second, it converts the normalized multiple-wavelength image data sets into relative changes in oxy-, deoxy-, and total hemoglobin levels. A flowchart of the sequence of **Image Recovery** operations is shown in Figure 4.

POST-PROCESSING

Post-processing comprises a collection of time-series analysis tools that can be applied to raw detector data sets, normalized detector data sets, and reconstructed image data sets. The operations in the **Signal Separation**, **Frequency Analysis**, **Correlation Analysis**, **Wavelet analysis** and **Rate Analysis** menus have been included in the current dynaLYZE version.

Signal Separation performs three main functions. The first two together constitute a blind source separation procedure [4]. The first step carried out is a principal component analysis (PCA) on the data set, or on a user-specified subset thereof. The second step is an extended temporal decomposition, via the algorithm of Molgedey and Schuster, which operates on a user-specified subset of the principal components. The third available operation is a general linear model (GLM) computation [4], which fits the detector-channel or image-pixel time series with any number of user-specified model functions. The GLM module automatically supplements these models with terms that account for constant offsets and linear and quadratic trends (drifts) in the data.

Frequency Analysis calculates Fourier transforms (See Figure 5(a),(b)) of selected data time series. Frequency filtering (Fig. 5(a),(b)) and region-of-interest capabilities also are provided. Both temporal and spatial views of the computed results are provided.

Correlation Analysis, with an interface similar to that for Frequency Analysis, calculates and displays results of cross-correlation, cross-spectral density (Fig. 5(c),(d)) and coherence computations for designated portions of data time series.

Wavelet Analysis performs a continuous Morlet wavelet analysis on user-specified data time series, and displays the results of the computation.

Rate Analysis provides several capabilities associated with rate calculations on selected data sets, including first derivative estimation via Savitzky-Golay filtering, curve fitting (polynomial, signal exponential and double exponential) and interval/time-delay analysis.

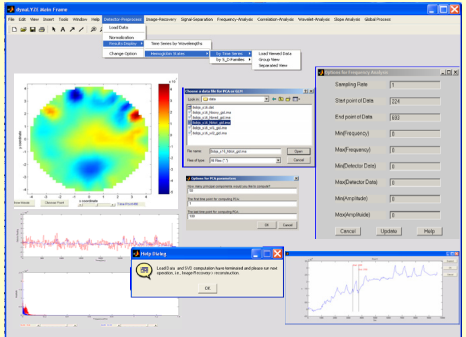

Figure 2. dynaLYZE GUIs

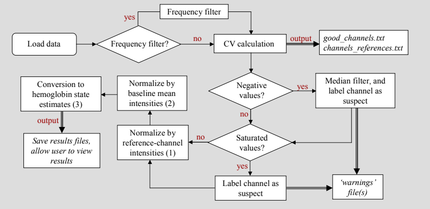

Figure 3. Flowchart of Detector Preprocess Operations

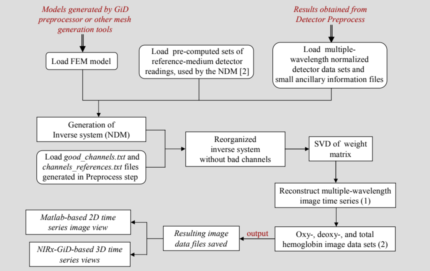

Figure 4. Flowchart of Image Recovery Operations

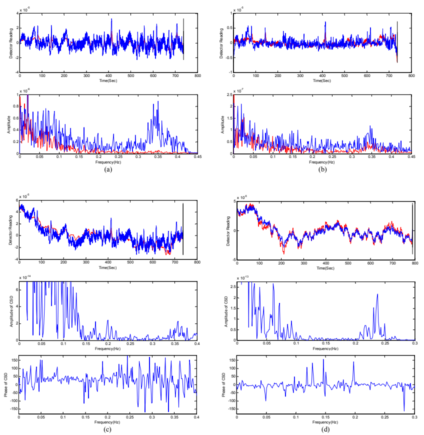

Figure 9. Examples of data post-processing operations performed with *dyna*LYZE. Data in 5(a)-(c) are derived from an dynamic optical mammography measurement conducted on a patient with bilateral breast cancer, which is responding to neoadjuvant chemotherapy preferentially on the *left* side. Data in 5(d) are derived from a healthy control participant in the same clinical study. In both cases, simultaneous dual-breast, two-wavelength measurements were performed; the specific results presented here are derived from the volume-averaged total hemoglobin (i.e., blood volume) signals for both the left (red curves) and right (blue curves) breasts. Fig. 5(a): top row = bandpass-filtered (0.005-0.43 Hz) mean Hb_{tot} time series, bottom row = amplitudes of the former curves' FTs, showing lower amplitude at most frequencies in the left breast, most notably in the respiratory frequency band (~0.32-0.4 Hz). Fig. 5(b): top row = bandpass-filtered time series of the spatial *standard deviation* of the Hb_{tot} signal, bottom row = amplitudes of the former curves' FTs, notably showing smaller left/right amplitude ratio in the respiratory frequency band than in 5(a). This indicates that the low amplitude in the left breast's mean signal arises from spatially heterogeneous phase of the respiratory frequency, not from its complete absence. Fig. 5(c): top row = low-pass-filtered (0-0.43 Hz) mean Hb_{tot} time series, middle row = amplitudes of the cross-spectral density (CSD) between the former curves, bottom row = corresponding CSD phase, which reveals a consistent 30°-40° phase difference between the left and right breasts. For comparison, the analogous results (mean Hb_{tot} time series, CSD amplitude, CSD phase) are shown for a healthy control subject in Fig. 5(d). Here the signals from both breasts are almost completely in phase at all frequencies; this type of response is typical for healthy subjects. (Close examination of the amplitude and phase curves in 5(c) and 5(d) reveals that the amplitude is essentially zero at those frequencies where the phase difference seemingly is large.)

A CLINICAL EXAMPLE: FUNCTIONAL NEUROIMAGING

Focal neuronal activation is expected to produce an event-related increase in blood flow, causing an increase in blood volume with improved oxygenation [5-6]. An example of our ability to record such responses from the head of an adult (motor cortex) in response to a box-car finger-tapping paradigm is shown in Figure 6. Illustrated is an event-related change in oxy-Hb levels paralleling the onset and cessation of finger tapping. Shown in Figure 7 are results from a similar experiment in which collected data were further processed to yield a spatial image of the response. Here we show the result obtained when the GLM technique was applied, with the boxcar design as the model function, to identify where in the image space this particular behavior was present. It is seen that the boxcar makes a significant contribution to the overall model fit in only a single, highly localized, region that isolated approximately 0.5-1.0 cm below the surface, a finding is consistent with results from fMRI studies.

Protocol for data collection and analysis:

- Instrumentation: A multichannel continuous wave (CW) near infrared (NIR) optical tomographic imager (DYNOT System, NIRx Medical Technologies, LLC., Glen Head, NY), operating at wavelengths of 760 nm and 830 nm, allows discrimination between oxyhemoglobin and deoxyhemoglobin concentrations.
- Subject: A single right-handed healthy adult female.
- Recording: Data were collected from 24 channels in parallel at a source switching rate of 2.5 Hz. 24 source-detector optodes configured in a rectangular pattern (8×6 cm) provided up to 576 independent detector channels. The rectangle was positioned over the left side of the head, approximately overlying the centro-temporal brain area.
- Task: After 320 seconds of rest with eyes closed, the subject alternated 3 block periods (~40 sec. each) of right hand four-finger flexion/extension, at 1 Hz, with 3 quiet resting blocks (~40 sec.).
- Data Pre-processing:
  - Low-pass filtering (0-0.15 Hz) and normalization of raw detector readings for the two wavelengths, where only data from channels with CV < 15% in the baseline time interval were used in subsequent steps.
  - Computation of changes in hemoglobin concentrations, according to a modified Lambert-Beer law, from the two wavelengths' time-series data.
  - One-tailed *t*-tests comparing motor versus rest, after linear & quadratic detrending, were carried out.
- Image Recovery:
  - Images of μ_a (absorption coefficient) were reconstructed, for both wavelengths.
  - Two-wavelength μ_a images were algebraically combined into spatial maps of the 3 forms of hemoglobin (oxy, deoxy, & total).
- Post Processing:
  - Time intervals corresponding to baseline and provocation (Activation/Rest) periods were selected.
  - Mean and standard deviation images for each time segment and each hemoglobin form were computed.
  - GLM analyses were performed on data from the two selected sub-intervals of time.

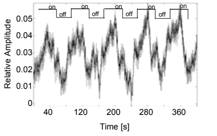

Figure 6. Temporal response of the oxy-Hb signal (first principal component) during finger-tapping sequence.

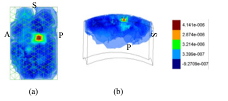

Figure 7. Each image is a spatial map of the coefficient for the GLM fit of the boxcar model function to the pixels' oxy-Hb time series. Two views are shown for the activation-rest time period. The *t*-statistics associated with largest positive and largest negative values of the GLM best-fit parameter are +9.25 ($p = 3.6\times10^{-19}$) and -7.09 ($p = 3.6\times10^{-12}$), respectively. A = anterior P = posterior, S = superior.

CONCLUSIONS

The dynaLYZE package provides a user-friendly interface and large numbers of integrated functions for data analysis, interrogation and visualization. These allow users to reorganize, image and interpret dynamic optical tomographic data sets produced by DYNOT system more conveniently and efficiently. The package will be further extended with more statistical modules in order to satisfy the requirements of different groups of users. Other extensions are also planned, relative to ROI analysis and surface and volume rendering of 3D data sets.

REFERENCES

[1] R. L. Barbour, H. L. Graber, Y. Pei, S. Zhong, and C. H. Schmitz, "Optical tomographic imaging of dynamic features of dense–scattering media," J. Opt. Soc. Am. A 18, 3018–3036 (2001).
[2] Y. Pei, H. L. Graber, and R. L. Barbour, "Influence of systematic errors in reference states on image quality and on stability of derived information for DC optical imaging," Appl. Opt. 40 5755–5769 (2001)
[3] Y. Pei, H. L. Graber, R. Barbour, "A fast reconstruction algorithm for implementation of time-series DC optical tomography," in Optical Tomography and Spectroscopy of Tissue V (Proceedings of SPIE, Vol. 4955), B. Chance, R. R. Alfano, B. J. Tromberg, M. Tamura, E. M. Sevick-Muraca, Eds., pp. 236–245 (2003). Copyright Society of Photo–Optical Instrumentation Engineers.
[4] H. L. Graber, Y. Pei, R. L. Barbour, D. K. Johnston, Y. Zheng, J. E. Mayhew, "Signal source separation and localization in the analysis of dynamic near–infrared optical tomographic time series," in *Optical Tomography and Spectroscopy of Tissue V (Proceedings of SPIE, Vol. 4955)*, B. Chance, R. R. Alfano, B. J. Tromberg, M. Tamura, E. M. Sevick-Muraca, Eds., pp. 31–51 (2003). Copyright Society of Photo–Optical Instrumentation Engineers
[5] G. Strangman, J. P. Culver, J. H. Thompson, and D. A. Boas, "A quantitative comparison of simultaneous BOLD fMRI and NIRS recordings during functional brain activation," *Neuroimage* **17,** 719-731 (2002).
[6] R. B. Buxton, *Introduction to Functional Magnetic Resonance Imaging: Principles and Techniques*, Cambridge University Press, Cambridge, (2002).

ACKNOWLEDGMENT

This research was support in part by the National Institutes of Health (NIH) under Grants R21-HL67387, R21-DK63692 and R41-CA96102 and by the US Army under Grant DAMD017-03-C-0018.

I look to ***THE DIFFUSION OF LIGHT*** and education as the resource to be relied on for ameliorating the condition, promoting the virtue, and advancing the happiness of man.

— Thomas Jefferson (1822)0